J Fluoresc (2008) 18:801–811
DOI 10.1007/s10895-007-0307-9

ORIGINAL PAPER

Non-invasive Near Infrared Fluorescence Imaging of CdHgTe Quantum Dots in Mouse Model

Haiyan Chen · Yunqing Wang · Jing Xu · Jinzi Ji · Jian Zhang · Yuzhu Hu · Yueqing Gu

Received: 23 September 2007 / Accepted: 6 December 2007 / Published online: 5 January 2008
© Springer Science + Business Media, LLC 2007

Abstract Near infrared CdHgTe quantum dots (QDs) acted as biomarker for in vivo imaging were synthesized in aqueous solution. The size and the fluorescence wavelength of the synthesized quantum dots can be arbitrary manipulated by using different refluxing time. In particular, the fluorescence wavelength was extended to near infrared range (700~900 nm), which make the in vivo imaging possible. Meanwhile, the characteristics, such as morphology, size, spectra, stability and toxicity were investigated. The dynamic bio-distribution, clearance from blood, liver and intestine in living animal were in vivo monitored by a NIR imaging system. The circulation of CdHgTe QDs in living mice was addressed semi-quantitatively according to the changes of fluorescence intensity. The high stability as well as high fluorescence intensity makes QDs particular interested candidates for in vivo imaging studies.

Keywords Near infrared · Quantum dots · Stability · In vivo · Fluorescence imaging

H. Chen · J. Zhang · Y. Gu (✉)
Department of Biomedical Engineering, School of Life Science and Technology, China Pharmaceutical University,
24 Shennong Road,
Nanjing 210009, People's Republic of China
e-mail: guyueqing@hotmail.com

H. Chen · Y. Wang · Y. Hu
Department of Analytical Chemistry, School of Basic Science, China Pharmaceutical University,
24 Shennong Road,
Nanjing 210009, People's Republic of China

J. Xu · J. Ji
Department of Pharmacy, School of Pharmaceutical Science, China Pharmaceutical University,
24 Shennong Road,
Nanjing 210009, People's Republic of China

Introduction

Current imaging techniques place more emphasis on functional monitor of tumor development, tracking metastases and observing the effects of therapeutics. Various magnetic resonance imaging (MRI) techniques (Over Hauser enhanced MRI [1, 2], Electron Paramagnetic Resonance Imaging [3] and Blood Oxygen Level-Dependent MRI [4]) have very prevalently application in clinic study, with a spatial resolution of a few millimeters and a temporal resolution in the order of a minute or more., Endoscope technique, such as gastroscope [5], enteroscope [6], is another way to ascertain the tumor sites. These endoscopes make patients suffering painful examination process [7]. Radioactive imaging methods, such as positron emission tomography (PET) and single photon emission computed tomography (SPECT) [8, 9], provide sensitivities beyond the nanomolar range, which makes these techniques attractive for in vivo imaging. However, the high cost as well as radioactive injection limits its widely application. Therefore, the development of a non-invasive cheap imaging technique will meet the need of practical application.

Optical imaging technique recently attractive more interest in the diagnostic process due to its easy operation, better temporal resolution and relative low cost. As all known, most tissue chromophores, including oxyhemoglobin, de-oxyhemoglobin and melanin, absorb comparatively weak in the near infrared (NIR) spectral range (700~900 nm) [10]. Therefore, NIR light possesses the advantage of penetrating living tissues several centimeters. Characterized with the deeper tissue penetration depth as well as non-radioactivity, NIR techniques have attracted extensively interest for in vivo real-time monitoring of biological signal in living tissues. In these years, NIR techniques

have been designed to diagnose disease [11, 12], monitor the response to therapeutic treatment [13, 14], evaluate the rehabilitation [15, 16] and so on. All the applications demonstrated optical imaging to be a promising monitor tool for in vivo imaging.

Due to the fact that most of the endogenesis lack the unique optical properties within the near infrared range, the extrinsic NIR fluorescent exogenous contrast agents make the in vivo study possible. Until recently, organic fluorophores were regularly introduced as exogenous contrast and the most commonly used agents are polymethines [17]. Peak excitation wavelength of this class is at 760–800 nm, and peak emission at 790–830 nm. However, organic fluorochromes have many disadvantages in the application of in vivo non-invasive optical imaging. They have narrow fluorescence excitation bands, wide and unsymmetrical fluorescence emission spectra, and severe photobleach, which is not stable enough to be monitored in vivo [18]. The photo-physical behavior of quantum dots (QDs) may offer a promising way to overcome most of these problems [19, 20]. QDs feature with many merits such as high quantum yields, narrow fluorescence emission band, very long effective Stokes shifts, high resistance to photo bleaching. It can provide several different emission colors using a single excitation wavelength [21, 22]. Synthetic routes of CdHgTe QDs in water was reported [23, 24], which showed much prospect because of their property of a large range of emissions wavelength in the NIR, tunable not only by size but also by different compositions.

In this study, CdHgTe QDs were synthesized in aqueous solution by a modified synthesized route. Their spectral properties, stability, toxicity were also studied. Moreover, the dynamic behaviors in different tissue/organs were investigated by using a mice model. In the same way, circulation of the QDs in mouse body was addressed semi-quantitatively according to the time-dependent changes of fluorescence intensity. and the blood clearance for this contrast agent has also been measured.

Materials and methods

Materials and instruments

The reagent $Cd(NO_3)_2$ (AR) was purchased from JinShanTing new chemistry agents company (shanghai, China) and used directly without further purification. Te powder and $NaBH_4$ were purchased from GuoYao chemistry agent corporation (Nanjing, China). Thioglycolic acid (TGA) was obtained from WanQing chemical agents corporation (NanJing, China) and Ethyl carbomate from QingXi Chemical Technology Company (Shanghai, China). BSA was obtained from Keygen Biotechnology (NanJing, China). Water for all reactions, solution preparation and polymer purification was double distilled.

PH meter (PHS-25) was purchased from Shanghai scientific instrument corporation (ShangHai, China). JEM-2100 transmittance electron microscope (Hitachi, Japan) was used to evaluate the morphology of particles. 754-PC UV–Vis spectrophotometer (JingHua technological instrument corporation, Shanghai, China) was used for UV–Vis spectra measurement. S2000 eight-channel optical fiber spectrographotometer (Ocean Optics corporation, America), a HL-2000-HP-FHSA halogen lamp (filter: 560±30 nm, Ocean Optics corporation, America) and a NL-FC-2.0–763 laser (λ=765.9 nm, nlight, China) light were utilized for fluorescence spectra detection.

Synthesis of thiol-stabilized CdHgTe QDs

CdHgTe QDs was synthesized by using a modified method referring to Harrison's report [24]. In details, 0.092 g of Cd $(NO_3)_2{\cdot}4H_2O$ was dissolved in 100 mL of water, and 60 μl of TGA (thiol stabilizer) was added under constant stirring, followed by adjusting the pH to the appropriate values by dropwise addition of 1 M solution of NaOH. The solution was placed in a three-necked flask and deaerated by N_2 bubbling for 30 min. Then, 600 μl freshly prepared NaTeH solution ((generated by the reaction of 0.04 g of Te powder, 0.06 g of $NaBH_4$ under and 1 mL of water under N_2 atmosphere) was added into the stirring reaction system. Meanwhile, 30 μl $Hg(NO_3)_2$ saturated solution was added into the system and bubbled with a slow nitrogen flow for another 30 minutes, which contributed to the red-shift to the near infrared range. CdHgTe precursors were formed at this stage, which is accompanied by a change of the solution color to brown. The precursors showed an absorption spectrum in NIR spectral region but no luminescence. Finally, the precursors were converted to CdHgTe QDs by refluxing the reaction mixture at 100 °C under open-air conditions. The thiol-capped CdHgTe QDs were obtained

Characterization of CdHgTe QDs in vitro

Structural characterization of thiol-capped CdHgTe QDs

To observe the morphology of CdHgTe QDs, TEM pictures of QDs were taken by JEM-2100 TEM. Briefly, diluted solution of CdHgTe QDs was dropped onto 400-mesh carbon-coated copper grids with the excessive solvent immediately evaporated before being loaded into the microscope for observation.

The absorbance spectra and emission spectra of CdHgTe quantum dots

Absorbance spectra of the synthesized CdHgTe QDs at different refluxing time (1 h, 4 h, 8 h and 12 h) were measured by UV–visible spectrophotometer.

Photoluminescence (PL) of CdHgTe QDs at different refluxing time (1 h, 4 h, 8 h and 12 h) were measured at room temperature by using a S2000 eight-channel optical fiber spectrographotometer equipped with a halogen lamp (filter: 560±30 nm).

Effect of pH on fluorescence intensity of CdHgTe QDs

Due to the pH sensitivity of QDs, fluorescence intensity of QDs solutions were measured in different pH conditions (2.9, 4.0, 4.9, 5.5, 6.1, 7.2, 8.3, 8.8, 9.5, 10.8, 11.6 and 12.1) by S2000 eight-gap optical fiber spectrographotometer equipped with a 765.9 nm laser light. NaOH solution (1 mol/L) and HCl solution (1 mol/L) were utilized to adjust the pH values.

Photostability of CdHgTe QDs in different medium

To investigate the photostability of CdHgTe QDs, CdHgTe QDs were dissolved in various medium (distilled water, plasma, blood, BSA solution and saline). A laser (λ= 765.9 nm, light intensity=26 mw) was utilized to continually irradiate the samples. The fluorescence intensity of these samples was measured at different time intervals within 2 hour by a S2000 eight-gap optical fiber spectrographotometer. Temperature for the measurements was kept at 37 °C.

Toxicity of CdHgTe QDs in mouse model

Kunmin mice, with 6–8 weeks old and about 20 g in weigh, were provided by China Pharmaceutical experiment animal center. All experiments were carried out in compliance with the Guide for the care and use of laboratory animals in China Pharmaceutical University.

The QDs solution was prepared by dissolving QDs in natural saline for intravenous injection. 25 mice were separated randomly into five groups (five mice in each group) and marked with No.0, No.1, No.2, No.3, No. 4. Natural saline as control was injected through the tail vein into the No.0 group mice. QDs (7 μg/g, 10.5 μg/g, 14 μg/g and 17.5 μg/g) were injected via tail vein into the No.1, No.2, No.3, No.4 group mice, respectively. The livability, living time, behavior and health of the mice in all groups were observed for three months.

Real time in vivo optical imaging of CdHgTe QDs in mouse model

Optical instruments

The need of real time observation of biological signals in living subjects has contributed to the establishment of NIR fluorescence imaging as an essential tool in biomedical and bioanalytical research laboratories. The instrumentation utilized to produce surface maps of the fluorescence signals in animals is simple and relatively cheap. Therefore, this sort of imaging system is prone to be accepted in most scientific research work.

The schematic diagram of NIR imaging system is shown in Fig. 1. For the fluorescence images, a NL-FC-2.0–763

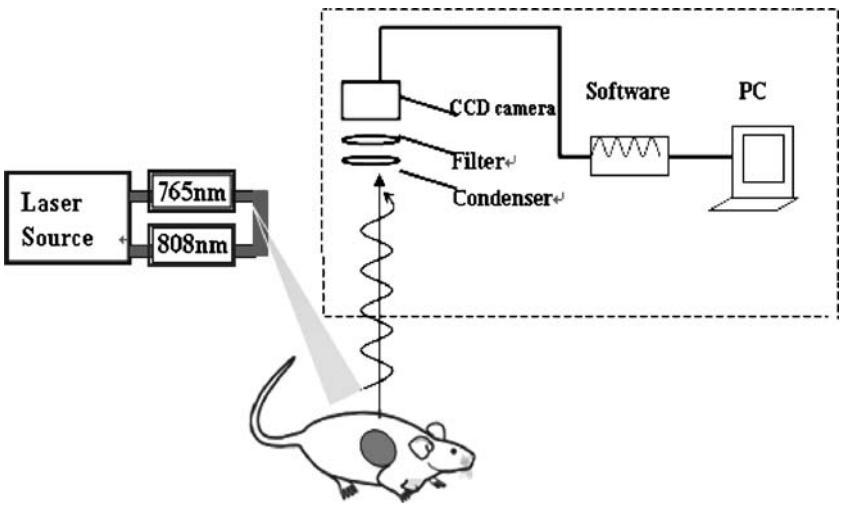

Fig. 1 Schematic diagram of NIR imaging system. A helium–neon laser (λ=765.9 nm) is defocused to provide a broad spot with even optical density, and another 808 nm laser is supplied as background light. High sensitivity CCD camera detects the reflected light, endogenously generated luminescence or fluorescence emission. An 800 nm long pass filter could blocked the laser light (765 nm) efficiently

laser (λ=765.9 nm) light was coupled into NIR optical fiber bundle and defocused to provide a broad spot with even optical density shining on the surface of the mouse. A high sensitive NIR CCD camera (Princeton, America) was positioned 10 cm above the subjects. An 800 nm long pass filter (Chroma, Rockingham, VT) was put ahead of the CCD to block the excitation and ambient light, and thus to capture the emitted fluorescence from the tissue. The imaging taking was controlled by the matched software. Besides, another HLU32F400 808 nm laser (LIMO, Dortmund, Germany) is supplied as background light to obtain the profile of the subjected animal (Otherwise, the imaging was completely black except the fluorescence spot).

In vivo optical imaging

The Mice (KM) were denuded by a mixture of Na_2S (5%) and starch followed immediately by daubing camphor ice to avoid further skin erosion. The denuded mouse was put back to the animal house and ready for experiment after 24 hours. Each mouse was anesthetized with an intraperitoneal (IP) injection of 150 μL ethyl carbamate (20 mg/mL) and then immobilized in a Lucite jig.

In a typical experiment, CdHgTe QDs aqueous solution (2 μg/g) was injected through the tail vein into each mouse. NIR imaging was then performed in a dark room on three mice by using the NIR imaging system. The light intensity of laser light from the fiber bundle was adjusted at 26 mw, which is the same as experimental condition indicated in the "Effect of pH on fluorescence intensity of CdHgTe QDs" section. For each mouse a background image (prior to injection) was firstly collected. A series of images were then collected at 10 s, 5 min, 30 min, 1 h, 2 h, 12 h and 24 h post-injection. The dynamic changes of QDs in different organs can be achieved by selecting the specific region of interest from the obtained imaging The subjected mouse was scarified And different organs were separated and washed by the natural saline and put together for fluorescence imaging.

Blood clearance

For fluorescence measurement of NIR QDs in blood, four mice were anesthetized with an intraperitoneal (IP) injection of 150 μL ethyl carbamate (20 mg/mL) and then immobilized in a Lucite jig. A 200 μL bolus of physiological saline was injected into the tail vein of mouse as control. CdHgTe QDs

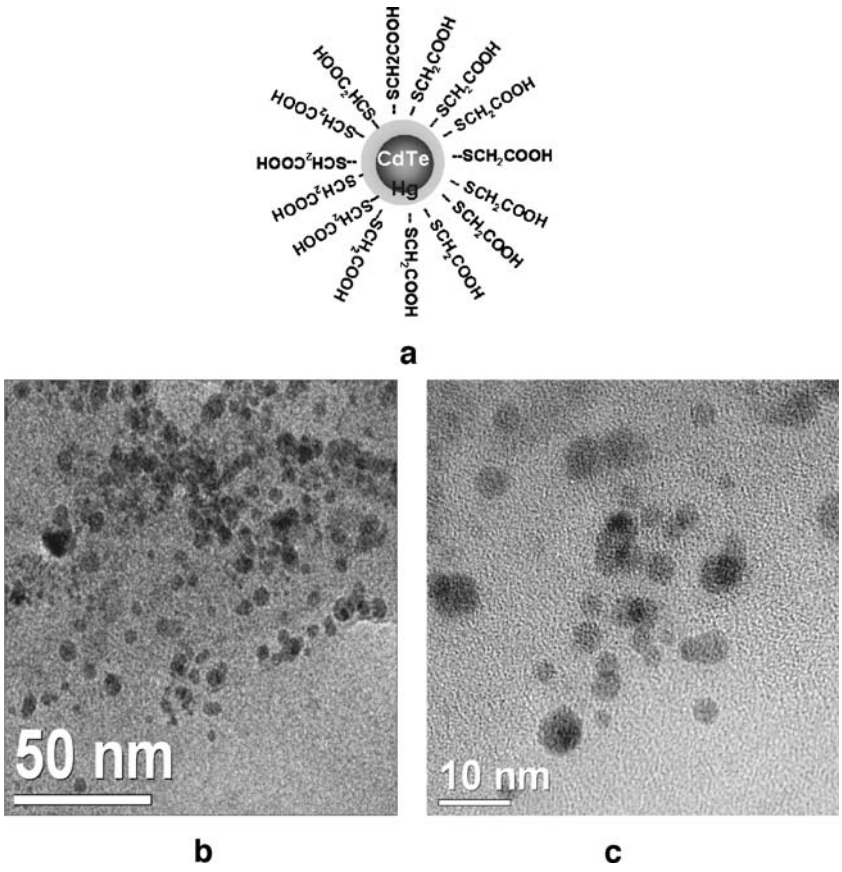

Fig. 2 (**a**) The structure diagram for CdHgTe QDs. The surface of CdHgTe QDs was coated with stabilizer (TGA). (**b**) Low resolution TEM images of TGA-capped CdHgTe QDs; (**c**) High resolution TEM images of CdHgTe QDs

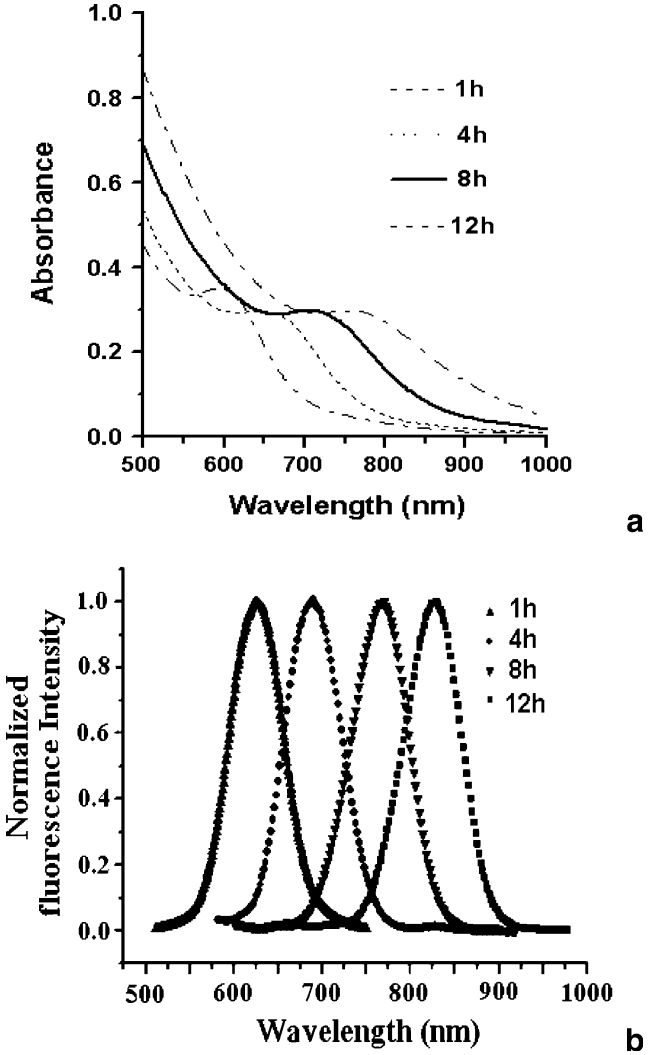

Fig. 3 (**a**) The UV–Vis absorbance spectra of CdHgTe QDs taken as prepared in different refluxing time (1 h, 4 h, 8 h and 12 h); (**b**): The PL spectra (λex=560 nm) of CdHgTe QDs taken as prepared in different refluxing time (1 h, 4 h, 8 h and 12 h)

(2 μg/g) were injected through the tail vein into the mice for blood clearance measurement. A series of 100 μL blood samples were collected from the eyeballs at the time interval of about 35 minutes over the first three hours and dropped onto the glass plate. The fluorescence was then measured using the same experimental approach as above. The feces was also collected for fluorescence measurement.

Results

Morphology and size of CdHgTe QDs

The structure of the synthesized QDs was shown in Fig. 2a. The surface of CdHgTe QDs was coated with stabilizer (TGA), and CdHgTe QDs has a structure similar to core/shell, CdTe as a core and Hg as a shell. Low-resolution TEM and high-resolution TEM (HRTEM) photos of thiol-capped CdHgTe QDs were taken. The representative photos shown in Fig. 2b and c indicate that the synthesized QDs (refluxing time=12 h) are close to sphericity and nearly mono-dispersed. The size of CdHgTe QDs was calculated from the TEM photos and was approximated 7 nm for this specific reaction condition.

The absorbance and emission spectra of CdHgTe QDs

Table 2 represented the change of CdHgTe size distribution as refluxing time extended. Actually, the particle size elevated with the increase of refluxing time, as shown in Table 2. CdHgTe QDs obtained the size of 2 nm, 4 nm, 5 nm and 7 nm, respectively, corresponding to the refluxing time of 1 h, 4 h, 8 h and 12 h. Obviously, the average size of CdHgTe QDs tends to be larger with prolongation of refluxing time.

Figure 3a and b show typical absorption and room-temperature PL spectra of CdHgTe QDs at different refluxing time of 1 h, 4 h, 8 h and 12 h. Spectra were measured in as-prepared CdHgTe colloidal solutions which were taken from the refluxing reaction mixture at designed intervals of time. A clearly resolved absorption maximum of the first electronic transition of CdHgTe QDs appears at 600 nm in 1 hour after refluxing. The absorption peaks shift to longer wavelength as the particles grow in the course of heating (Fig. 3a). 760 nm absorption peak was obtained after refluxing 12 h. Experiment indicated that the absorption peak cannot be extended over 900 nm in certain feed ratio composition no matter how long the refluxing time was. The PL bands (Fig. 3b) are close to the absorption thresholds (so called band-edge photoluminescence) and are sufficiently narrow with full width at half-maximum (FWHM) of 50–70 nm. Fluorescence maximum

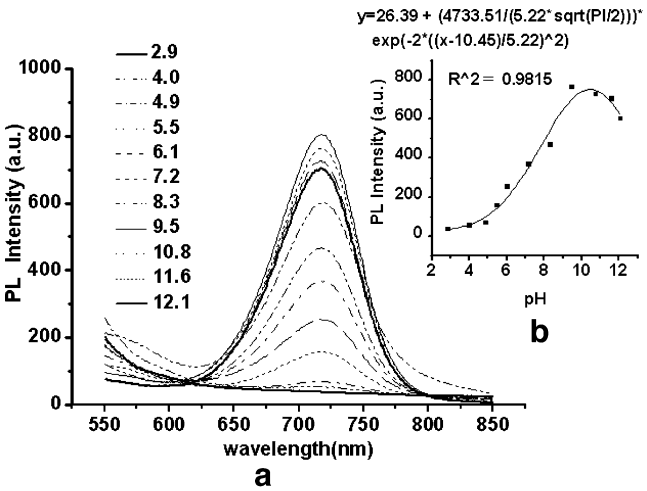

Fig. 4 (**a**) Emission spectra of CdHgTe QDs at different pH conditions. (**b**) Fluorescence intensity of CdHgTe QDs plotted against pH values

at 625 nm appears 1 h after refluxing when the CdHgTe nanocrystals reach the size of 4 nm. whereas PL maximum at 830 nm.(FWHM=70 nm) was obtained after 12 h refluxing with 7 nm nanocrystal. The other spectral range was located between these two wavelengths.

Relationship between pH and PL intensity of CdHgTe QDs

Figure 4 shows the relationship between pH and PL intensity of CdHgTe QDs. As shown in Fig. 4, fluorescence intensity went through obvious change when pH value varied. The highest fluorescence intensity occurred when pH value was approximated to 9. When pH value was higher or lower than this critical value, it resulted in decrease of fluorescence intensity. When pH was in the range of 2.9–4.9, fluorescence quenching occurred.

Photostability study of CdHgTe QDs in aqueous solution, plasma, blood, BSA solution and saline

Figure 5 shows photostability of CdHgTe QDs in different medium (aqueous solution, plasma, blood, BSA solution and saline) under irradiation with 765 nm laser light in 100 min. The fluorescence intensity of CdHgTe QDs almost remains the same as original value when irradiation time of laser light (765 nm) extended to 100 minutes, which suggests excellent stability of CdHgTe QDs in different biological environment. Moreover, colloidal solutions of CdHgTe QDs could maintain their optical properties after several months' exposure to the air at room temperature.

Study on toxicity of CdHgTe QDs in mouse model

Toxicity of CdHgTe QDs studied in mouse model is shown in Table 1. Life time is defined as the alive time of experiment mice, and livability is defined as the ratio of living mice versus total mice in the same group during the experimental period (3 months). As shown in Table 1, No.1 and No.2 group mice were still alive 3 months after injection of QDs with lower dose (7 μg/g) and didn't show any symptom such as ache, illness and abnormal behavior. Whereas mice in group No.3 and No.4 died 24 hours and 8 hours respectively after injection of QD at higher dose (14 μg/g and 17.5 μg/g). The safe maximum dose in these cases was found at the dose of 10.5 μg/g. Results indicated there is no special toxicity to the mice when the dosage of CdHgTe QDs was controlled in a safe range.

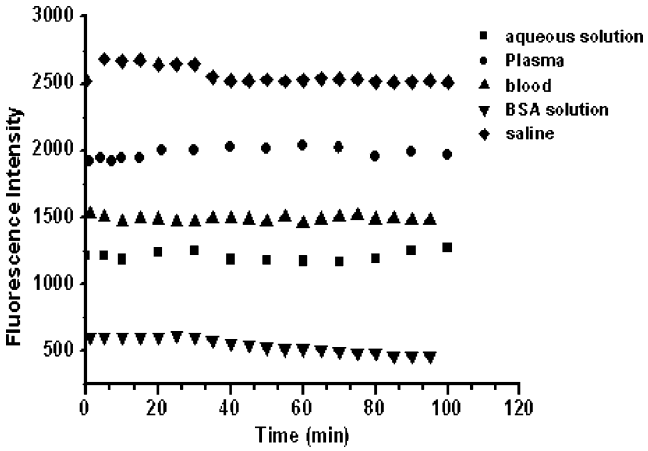

Fig. 5 Photostability of CdHgTe QDs in different medium (aqueous solution, plasma, blood, BSA solution and saline) under irradiation with 765 nm laser light in 100 min

In vivo imaging

Figure 6 represents a series of in vivo images taken by the NIR imaging system at different time interval after QDs injection. The fluorescent background prior to QDs injection was firstly acquired (Fig. 6a). After CdHgTe QDs (2 μg/g) was injected through the tail vein, fluorescence images of the mouse was acquired at 1 min, 1 hour, 3 hour, 5 hour and 8 hour (Fig. 6b,c,d,e,f). Photos indicated that QDs immediately distributed to all over the vessels by blood circulation after tail vein injection of QDs. The dynamic changes of CdHgTe QDs in the superficial vessels were clearly observed. Moreover, a network of blood vessels could be distinguished in the fluorescence images (Fig. 6b). Although some of the vessels observed in the imaging were from superficial skin layer, other deeper vessels also still presented in the network, which was confirmed by the skin dissection.. In the experiment, the injection process could be observed as soon as the QDs entered the tail vein (image was not shown). And then, QDs were observed to arrive immediately at liver tissue within 30 second, One hour later, CdHgTe QDs entered into intestine and cleared from this tissue within several hours. The fluorescence signals disappeared in the mouse body completely 8 hours after QDs injection, CdHgTe QDs passed through femoral veins in the mouse was conspicuously observed when the excitation light was focused on the two legs, as shown in Fig. 6g and h.

Given the spectral characteristics of the QDs and the sensitivity of the instrumentation, NIR imaging technique is well suitable for pharmacokinetic analysis. The dynamic changes of QDs in different organs can be acquired by selecting the specific region of interests (ROIs) from the obtained imaging. Figure 7a and b presents analyzed data of CdHgTe QDs from liver tissue as well as intestine tissue. In each case, the background fluorescence, as measured before injection of the QDs, has been subtracted. The fluorescent intensities in ROIs for liver and intestine tissue were averaged and then plotted against with the time. The elimination of CdHgTe QDs from liver and intestine tissue was fitted with an exponential form (y=565.97 exp (−0.5611x), R^2=0.9500) and a polynomial form ($y = 80.59 - 2.35x +$

Table 1 Toxicity of CdHgTe QDs studied in mouse model

Group number	Injection dose (μg/g)	Livability in 3 months (%)	Living time	Behavior/ health
No. 0	0	100	Long-time	Normal
No. 1	7	100	Long-time	Normal
No. 2	10.5	100	Long-time	Normal
No. 3	14	0	24 h	Died
No. 4	17.5	0	8 h	Died

Life time is defined as the time for experiment mice to live, and livability is defined as the ratio of living mice versus total mice during the experimental period

$0.05\bar{x}^2 - 4.00x^3 - 7.00x^4$, R^2=0.7899), which were shown in Fig. 7a,b, respectively (The data of fluorescence intensity in the liver and intestine were obtained from the mice images shown in Fig. 6).

To validate the information collected from in vivo fluorescence images, the mice were performed a thoracotomy and the fluorescence image was taken on the parallel experiment mouse. Figure 6i is image from the thoracotomy mouse at the time corresponding to Fig. 6e. Fluorescence signals appeared in the liver and intestine tissues (the needle pointed), which was consistent with the fluorescence image shown in Fig. 6e. Then, the major organs (liver, heart, spleen, kidney and lung) of the mouse were separated and the fluorescence image was acquired, which was shown

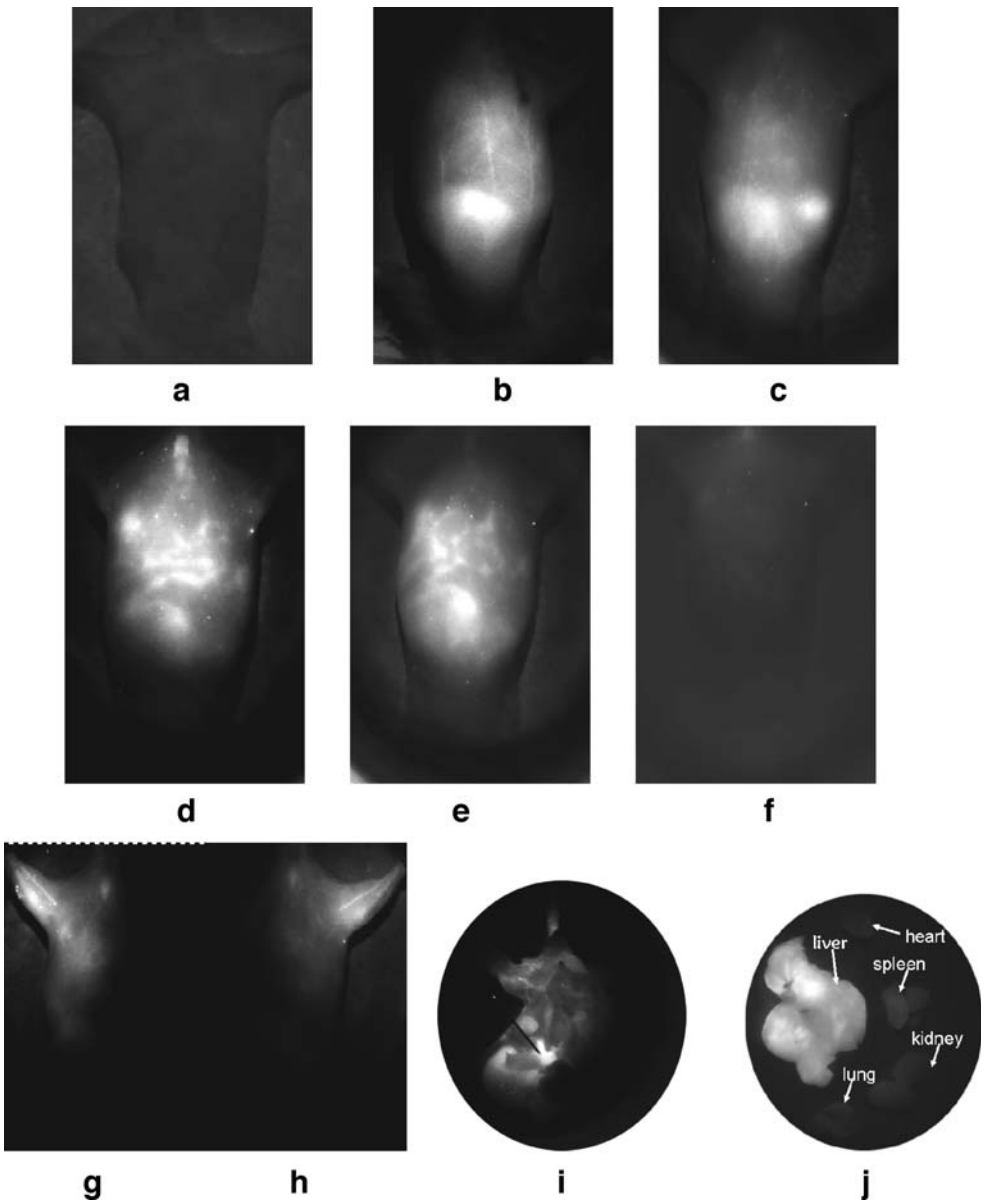

Fig. 6 A series fluorescence images of the mouse after CdHgTe QDs was injected via tail vein. (**a**) the fluorescent background measured by 765 nm excitation prior to QDs injection; (**b**) Fluorescence image of the same mouse approximately 1 min; (**c**) 1 h; (**d**) 3 h; (**e**) 5 h; (**f**) 8 h after 100 μL of CdHgTe QDs was injected; (**g**) Fluorescence image of the left leg; (**h**) the right leg of the mouse approximately 30 s after 100 μL of CdHgTe QDs was intravenous injected through the tail; (**i**) fluorescence image of the mouse taken after performing a thoracotomy at the time corresponding to (**e**); (**j**) The mouse was executed 5 h later. The major tissues of the mouse were removed and the fluorescence image was taken

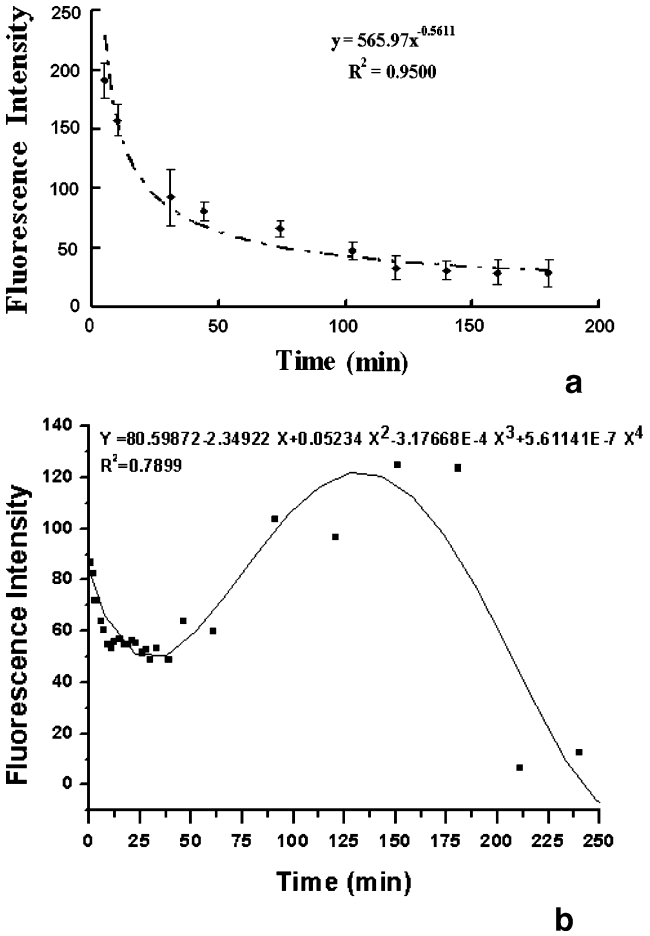

Fig. 7 The background fluorescence, as measured before QDs injection, has been subtracted. (**a**) Fluorescence intensity in intestine region of interest was acquired at regular time intervals after CdHgTe QDs injected; (**b**) Fluorescence intensity in small liver region of interest was acquired at regular time intervals after CdHgTe QDs was injected. The fluorescence intensity in ROI was averaged and plotted against time

in Fig. 6j. Fluorescence intensity in the liver was strong enough to be distinguished from other tissue sites (heart, spleen, kidney, and lung).

Blood clearance

Blood samples were drawn from eyeball at regular intervals after QDs injection for three mice. Figure 8 represents the fluorescence intensity of the blood sample at a typical mouse. The data was fitted with an exponential formulation (y=295.67 exp (−0.0099x), R^2=0.9964), as shown in Fig. 8.

Discussion and conclusion

In this study, nanocrystal CdHgTe were successfully synthesized and manipulated in terms of size and emission wavelength. In the refluxing or heating process, nanocrystal of CdHgTe was growing. And thus, the size of CdHgTe QDs increased with the extension of refluxing time at a certain temperature (Table 2). In our experiment, the reaction temperature was fixed at 100 °C, and the composition of the CdHgTe QDs was kept the same in order to study the influence of reaction time on size and optical properties of CdHgTe QDs.

UV–Vis spectrum is most commonly used in the study of the structure and other properties of semiconductor QDs. In the region of the UV and Visible energy band, transition of free electron from valence band to conduction band is the main reason that causes strong and wide absorption region [25, 26]. When the size of semiconductor reduced to nanometer grade, the energy band-gap depends on the size of quantum dots. It is always true that the smaller the size is, the larger the energy band-gap is. In this way, the emission wavelength can be adjusted by choosing different size, which is controlled by the reaction time, composition and so on. The process of reaction could be observed by the color of QDs solution and also could be verified by UV–Vis and fluorescence spectra [27, 28]. The absorption range of QDs is wide, which leads to the wide excitation wavelength coverage. In this way, QDs of different size could be excited by single wavelength. All samples in our experiments showed a well-resolved absorption maximum, indicating a sufficiently narrow size distribution of the CdHgTe QDs. The emission spectra of QDs in the NIR region are usually much broader than those in the blue and visible regions [24]. However, the emission spectra of the CdHgTe QDs prepared by our method are narrow and symmetric. The fwhm (about 50–70 nm) is obviously narrower than that of CdHgTe QDs prepared according to the reported approach (about 200 nm) [24, 29]. The longer wavelengths shift to NIR range with increasing size of the nanocrystals, which means that the band gap of CdHgTe

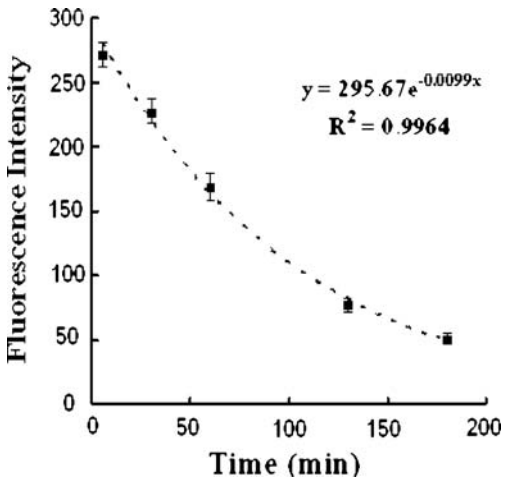

Fig. 8 The background fluorescence, as measured before QDs injection, has been subtracted. Fluorescence intensity of blood drawn from the mice eyeball at regular time intervals after CdHgTe QDs was injected

Table 2 The change of CdHgTe size distribution as refluxing time extended

Compound	CdHgTe QDs			
Refluxing time (h)	1	4	8	12
Size (nm)	2	4	5	7

CdHgTe QDs obtained the size of 2 nm, 4 nm, 5 nm and 7 nm, respectively, corresponding to the refluxing time of 1 h, 4 h, 8 h and 12 h

becomes narrower with the growth of the QDs, was a consequence of the quantum confinement [30].

Due to the excellent optical characterization of QDs, it is easy to distinguish and recognize different protein molecules by labeling QDs of different sizes to them. Single excitation wavelength could be selected to acquire the whole emission spectra information of these different protein molecules. In process of studying the dynamic behavior of biological signals, the background autofluorescence interference could be avoided by using the specific excitation wavelength.

Although antibody conjugated polymer-encapsulated QD probes was reported to be efficacy for cancer targeting [31], QDs emitting in the visible range is not optimal for in vivo imaging because of the high absorption of the tissue and thus the low detecting sensitivity. To improve visualization and resolution for in vivo imaging, QDs should have emission wavelength shift to NIR range for less absorption and deeper penetration depth.

TGA is a kind of weak acid whose water dissolubility depends on its dissociation in different pH environment. TGA was ionized in alkaline condition and thus enhanced the water dissolubility of CdHgTe QDs due to the surface of CdHgTe QDs coated with TGA. High fluorescence intensity of thiol-capped QDs occurred in alkaline environment (usually pH~9) for higher solubility of QDs in this condition, Deionization of TGA increased greatly when pH changed from 2.9 to 4.9, which destroyed the interaction between thiol group and CdHgTe QDs. Then, CdHgTe QDs sediment was observed in the bottom of reaction flask. Extension of the clever mechanisms (pH sensitivity) of quantum dots would in principle offer the opportunity to develop a new generation of luminescence chemosensors with superior luminescent properties [32].

Our thiol-capped CdHgTe QDs has a structure similar to core/shell. The mercury shell with wide band-gap was grown on the surface of the core (CdTe), eliminating the surface traps which weaken the nonradiative effect. This less trapped core/shell structure results in higher stability and increased brightness of CdHgTe QDs. TGA addition also contributes to the stability of CdHgTe QDs. The merit of high stability features obvious advantage for long-term observation in the NIR imaging and make the possibility of quantitatively pharmacological study. Moreover, the photostability of QDs could be designed to long-time observation of different biological molecules in cells, pharmacological properties of the drug as well as for long time fluorescence image of biological tissues in different deep layers. The same meaning.

The potential toxic effects of inorganic QDs have recently become a hot issue in the application of QDs in human study. The toxic study is complicated due to the variety of synthetic routes, solvent-dependent solubility, functionalized surface groups and so on. At higher concentrations, noticeable effects on embryo development were reported [33, 34]. Although QDs are not completely innocuous, they can accomplish their task without major interference with the function of the body within the safe range, as showed in Table 1. Moreover, QDs with a stable polymer coating have been reported to be essentially nontoxic to cells and animals, whereas breaking down of protective coating leads to cell damage and death [35], which is especially useful in targeted therapy. The less protected the core or core/shell nanocrystal is, the faster the effects appear to cell viability or function with the release of Cd^{2+} or Te^{2+} ion [36]. Toxicants that impair normal reproductive functions are an important public health issue, which needs to be further studied. Study of the cellular toxicity and in vivo degradation mechanisms of CdHgTe QD probes will be our urgent direction.

Although 10.5 μg/g is the maximum dose for the safe application (as shown in Table 1), 2 ug/g injection was selected, which greatly reduce the toxicity of QDs in animal subject while obtaining enough signal. (Fig. 5). As for the optimal dose and toxicity of CdTeHg QDs, injection of 2 μg/g CdTeHg QDs did not exhibit significant toxicity, and no abnormal behavior of the mice was observed in all of the in vivo imaging experiments. A key question is whether QDs can be used directly in clinical phase. Although we did not observe any toxicity when the injection dose was controlled below 10.5 μg/g, integrate cellular toxicity studies and complete in vivo toxicology still need to be performed before any application in humans.

For in vivo imaging, QDs must have adequate stability in biological environment, No aggregation was observed for CdHgTe QDs in our experiment, likely because of the highly hydrophilicity and higher stability of CdHgTe QDs. In the imaging process, high accumulation of QDs in liver was observed immediately after QDs injection (10 s post injection), indicating that the mononuclear phagocytes of the RES were involved in the clearance of some of the circulating QDs in the mice. The bio-distribution pattern showed long time retention in the intestine (Fig. 6). This finding may attribute to the macromolecular-based pharmacomodulation, meaning that the metabolism and elimina-

tion of QDs significantly via liver–intestine circulation. The ex-vivo organ biodistribution (Fig. 6i and j) confirmed this circulation pattern. Moreover, the fluorescence signal in feces (data not shown) further confirmed that most of QDs eliminate via intestine but not kidney. These data also indicated that toxicity of QDs could be reduced by their elimination from the biology bodies.

To confirm the observed fluorescence decrease attributing to the elimination of QDs from tissue rather than fluorescence quenching, the fluorescence intensity of a blood-QDs mixture was monitored with the sample continuously exposure to 26 mw laser light for 100 minutes. The data demonstrated that CdHgTe QDs are reasonably stable under physiological conditions, no photobleaching occurred. The relatively slow elimination of CdHgTe QDs from intestine tissue was observed when compared to blood and liver tissue. Furthermore, the elimination curve of QDs in intestine tissue is different from blood and liver tissue, which suggests the overlap of the intestine tissue and confirmed by the back-forth movement of QDs signal in intestine. The combination of NIR imaging technique and NIR fluorescence probe permits the measurement of pharmacokinetics over a long period. Further experiments are needed for the dynamic behavior of CdHgTe QDs in mouse model.

In summary, the CdHgTe QDs characterized by excellent optical property, less photo-bleaching and biocompatible were synthesized in aqueous phase. It has been proven to be a useful fluorescent angiographic contrast agent in the NIR range. preliminary experiments and analyses demonstrated the feasibility to study the pharmacokinetics associated with CdHgTe QDs.

More extensive studies could be performed to characterize the elimination of this semiconductor QDs in other animal models. The use of proper shell functional groups as well as the establishment of covalent bonding with other agents (such as antibody, targeting peptide, small specific molecules and so on) may offer a promising way to target this and other QDs to specific tissues, diagnose and therapy of diseases.

Acknowledgments The authors are grateful to Natural Science Foundation Committee of China (NSFC30672015, NSFC03030103), the Ministry of Education of China and China Pharmaceutical University for their financial supports.

References

1. Bharucha DX, Campbell TB, Valencia I, Hardison HH, Kothare SV (2007) MRI findings in pediatric ophthalmoplegic migraine: a case report and literature review. Pediatr Neurol 37(1):59–63
2. Kim JY, Lee J, Han JK, Kim SH, Lee JY, Choi JY, Kim SJ, Kim HJ, Kim KH, Choi BI (2007) Contrast-enhanced MRI combined with MR cholangiopancreatography for the evaluation of patients with biliary strictures: differentiation of malignant from benign bile duct strictures. J Magn Reson Imaging 26(2):304–312
3. Borel A, Laus S, Ozarowski A, Gateau C, Nonat A, Mazzanti M, Helm L (2007) Multiple-frequency EPR spectra of two aqueous Gd3+ polyamino polypyridine carboxylate complexes: a study of high field effects. J Phys Chem A 111(25):5399–5407
4. Roberts C, Tran TT, Song AW, Woldorff MG (2007) Component structure of event-related fMRI responses in the different neurovascular compartments. Magn Reson Imaging 25(3):28–334
5. Bergström M, Swain P, Park PO (2007) Measurements of intraperitoneal pressure and the development of a feedback control valve for regulating pressure during flexible transgastric surgery (NOTES). Gastrointest Endosc 66(1):174–178
6. Hekmat H, Al-toma A, Mallant MP, Mulder CJ, Jacobs MA (2007) Usefulness of the double-balloon enteroscope in colonoscopies performed in patients with previously failed colonoscopy. Scand J Gastroenterol 42(2):277–278
7. Kimura T, Muguruma N, Ito S, Okamura S, Imoto Y, Miyamoto H, Kaji M, Kudo E (2007) Infrared fluorescence endoscopy for the diagnosis of superficial gastric tumors. Gastrointest Endosc 66 (1):37–43
8. Winnard P, Raman V (2007) Real time non-invasive imaging of receptor–ligand interactions in vivo. J Cell Biochem 90(3):454–463
9. Kubo N, Zhao S, Fujiki Y, Kinda A, Motomura N, Katoh C, Shiga T, Kawashima H, Kuge Y, Tamaki N (2005) Evaluating performance of a pixel array semiconductor SPECT system for small animal imaging. Ann Nucl Med 19(7):633–639
10. Derfus AM, Chen AA, Min DH, Ruoslahti E, Bhatia SN (2007) Targeted quantum dot conjugates for siRNA delivery. Bioconjug Chem 18:1391–1396
11. Furukawa T, Sato H, Shinzawa H, Noda I, Ochiai S (2007) Evaluation of homogeneity of binary blends of Poly(3-hydroxybutyrate) and Poly(L-lactic acid) studied by Near Infrared Chemical Imaging (NIRCI). Anal Sci 23(7):871–876
12. Wessels JT, Busse AC, Mahrt J, Dullin C, Grabbe E, Mueller GA (2007) In vivo imaging in experimental preclinical tumor research—A review. Cytometry A 71A(8):542–549
13. LeMaire SA, Ochoa LN, Conklin LD, Widman RA, Clubb FJ Jr, Undar A, Schmittling ZC, Wang XL, Fraser CD Jr, Coselli JS (2006) Transcutaneous near-infrared spectroscopy for detection of regional spinal ischemia during intercostal artery ligation: preliminary experimental results. J Thorac Cardiovasc Surg 132 (5):1150–1155
14. Tachtsidis I, Tisdall M, Leung TS, Cooper CE, Delpy DT, Smith M, Elwell CE (2007) Investigation of in vivo measurement of cerebral cytochrome-c-oxidase redox changes using near-infrared spectroscopy in patients with orthostatic hypotension. Physiol Meas 28(2):199–211
15. Strangman G, Goldstein R, Rauch SL, Stein J (2006) Near-infrared spectroscopy and imaging for investigating stroke rehabilitation: test–retest reliability and review of the litemouseure. Arch Phys Med Rehabil 87(12):12–19
16. Okamoto M, Dan H, Shimizu K, Takeo K, Amita T, Oda I, Konishi I, Sakamoto K, Isobe S, Suzuki T, Kohyama K, Dan I (2004) Multimodal assessment of cortical activation during apple peeling by NIRS and fMRI. Neuroimage 21(4):275–288
17. Hales JM, Zheng S, Barlow S, Marder SR, Perry JW (2006) Bisdioxaborine polymethines with large third-order nonlinearities for all-optical signal processing. J Am Chem Soc 128(35):11362–11363
18. Michalet X, Pinaud FF, Bentolila LA, Tsay JM, Doose S, Li JJ, Sundaresan G, Wu AM, Gambhir SS, Weiss S (2005) Quantum dots for live cells, in vivo imaging, and diagnostics. Science 307:538–544
19. Qian J, Yong KT, Roy I, Ohulchanskyy TY, Bergey EJ, Lee HH, Tramposch KM, He S, Maitra A, Prasad PN (2007) Imaging

pancreatic cancer using surface-functionalized quantum dots. J Phys Chem B 111(25):6969–6972
20. Basabe-Desmonts L, Reinhoudt DN, Crego-Calama M (2007) Design of fluorescent materials for chemical sensing. Chem Soc Rev 36(6):993–1017
21. Lee SF, Osborne MA (2007) Photodynamics of a single quantum dot: fluorescence activation, enhancement, intermittency, and decay. J Am Chem Soc 129(29):8936–8937
22. Archer PI, Santangelo SA, Gamelin DR (2007) Inorganic cluster syntheses of TM(2+)-Doped quantum dots (CdSe, CdS, CdSe/CdS): physical property dependence on dopant locale. J Am Chem Soc 129(31):9808–9818
23. Han H, Sheng Z, Liang J (2007) Electrogenerated chemiluminescence from thiol-capped CdTe quantum dots and its sensing application in aqueous solution. Anal Chim Acta 596(1):73–78
24. Harrison MT, Kershaw SV, Burt MG, Eychmuller A, Weller H, Rogach AL (2000) Rogach. Wet chemical synthesis and spectroscopic study of CdHgTe nanocrystals with strong near-infrared luminescence. Mater Sci Eng B 69–70:355–360
25. Huynh WU, Dittmer JJ, Alivisatos AP (2002) Hybrid nanorod-polymer solar cells. Science 295:2425–2427
26. Klimov VI, Mikhailovsky AA, Xu S, Malko A, Hollingsworth JA, Leatherdale CA, Eisler HJ, Bawendi MG (2000) Optical gain and stimulated emission in nanocrystal quantum dots. Science 290:314–317
27. Murray CB, Norris DJ, Bawendi MG (1993) Synthesis and characterization of nearly nonodisperse CdE (E=S, Se, Te) semiconductor nanocrystallites. J Am Chem Soc 115:8706–8715
28. Smith AM, Nie S (2004) Chemical analysis and cellular imaging with quantum dots. Analyst 129:672–677
29. Rogach AL, Harrison MT, Kershaw SV, Kornowski A, Burt MG, Eychmuller A, Weller H (2001) Colloidally prepared CdHgTe and HgTe quantum dots with strong near-infrared luminescence. Phys Status Solidi B 224:153–158
30. Michalet X, Pinaud FF, Bentolila LA, Tsay JM, Doose S, Li JJ, Sundaresan G, Wu AM, Gambhir SS, Weiss S (2005) Quantum dots for live cells, in vivo imaging, and diagnostics. Science 28:538–544
31. Gao X, Cui Y, Levenson RM, Chung LWK, Nie S (2004) In vivo cancer targeting and imaging with semiconductor quantum dots. Nat Biotechnol 22(8):969–976
32. Tomasulo M, Yildiz I, Kaanumalle SL, Raymo FM (2006) pH-sensitive ligand for luminescent quantum dots. Langmuir 22 (24):10284–10290
33. Hardman R (2006) A toxicologic review of quantum dots: toxicity depends on physicochemical and environmental factors. Environ Health Perspect 114:165–172
34. Lovric J, Cho SJ, Winnik FM, Maysinger D (2005) Unmodified cadmium telluride quantum dots induce reactive oxygen species formation leading to multiple organelle damage and cell death. Chem Biol 12:1227–1234
35. Derfus A, Chen W, Bhatia S (2004) Probing the cytotoxicity of semiconductor quantum dots. Nano Lett 4:11–18
36. Cho SJ, Maysinger D, Jain M, Röder B, Hackbarth S, Winnik FM (2007) Long-term exposure to CdTe quantum dots causes functional impairments in live cells. Langmuir 23(4):1974–1980